Properties of a separable representation of optical potentials

M. Quinonez,[1,2] L. Hlophe,[1,2,3] and F. M. Nunes[1,2,*]
[1]*National Superconducting Cyclotron Laboratory, Michigan State University, East Lansing, Michigan 48824, USA*
[2]*Department of Physics and Astronomy, Michigan State University, East Lansing, Michigan 48824-1321, USA*
[3]*Lawrence Livermore National Laboratory, L-414, Livermore, California 94551, USA*

(Received 27 April 2020; accepted 22 July 2020; published 7 August 2020)

Background: Separable interactions have a long history in nuclear physics. In the last few years, separable expansions have been used to represent the optical potential between a nucleon (proton or neutron) and a target.
Purpose: We explore the nonlocal properties of these separable optical potentials as well as their convergence behavior.
Method: For a couple of cases, we use the generalized Ersnt-Shakin-Thaler scheme to generate separable interactions starting from local optical potentials. We study the variation of the interaction with energy range and rank.
Results: We find that, overall, the off-diagonal behavior of the converged separable interaction deviates from the Gaussian form assumed by Perey and Buck [F. Perey and B. Buck, Nucl. Phys. **32**, 353 (1962)]. However, in the region surrounding the maximum depth the Gaussian form works quite well. Focusing on this region, we study potentials describing neutron elastic scattering on ^{16}O and ^{48}Ca for beam energies in the range of $E = 10$–50 MeV and explore several measures of nonlocality of the separable interactions.
Conclusions: When the energy range considered for generating the separable interaction is $0 \leqslant E_{\text{range}} \leqslant 50$ MeV, the resulting nonlocality is large and target dependent. Contrarily, the nonlocality obtained including larger energy ranges in the separable procedure is independent of the target and other details of the original local potential. We find that, even when including in the expansion many support points with energy ranges $0 \leqslant E_{\text{range}} \leqslant 2400$ MeV, the resulting potential retains nonlocal behavior. Connections with microscopic optical potentials as well as other transformations used in the nucleon-nucleon domain are made.

DOI: 10.1103/PhysRevC.102.024606

I. INTRODUCTION

One of the greatest challenges in the physics of nuclei concerns the interactions themselves. Effective interactions are developed to incapsulate the many degrees of freedom contained in the system. Much work has been devoted to the development of both nucleon-nucleon effective interactions [1], the so-called *NN* force, and nucleon-nucleus effective interactions, referred to as optical potentials (e.g., Refs. [2–4]). In this work we focus on the latter and in particular on their properties when represented in separable form.

In the past, *NN* forces were derived phenomenologically with different levels of complexity (e.g., AV18 [5] and Minnesota [6]). In the last two decades the field has shifted toward generating these interactions in a more controlled fashion through effective-field theory (EFT) [7]. Different transformations on *NN* forces have also been proposed to enable greater efficiency when used in many-body problems: these include $V_{\text{low}k}$ [8,9] and similarity renormalization group methods [10]. In both of these examples high-momentum components of the interaction are shifted to low-momentum off-diagonal behavior, while preserving the on-shell properties of the interaction. When analyzed in coordinate space, these transformations induce nonlocality properties that do not affect the two-body observables but can have an impact in three- and more-body calculations. As is discussed here, a similar situation can occur when considering nucleon-nucleus optical potentials.

Separable interactions have a long history in few-nucleon physics (e.g., Refs. [11–13]). Because the three-body Faddeev equations in momentum space [14] simplify greatly when using separable interactions, this approach was originally very popular. As computational capabilities increased, the few-nucleon field evolved to using more realistic nonseparable interactions (e.g., Refs. [15,16]). The complications introduced by the infinite-range Coulomb force in the three-nucleon problem were handled separately by screening and renormalization techniques [17].

For over a decade, the few-nucleon techniques have been ported into nuclear reactions and in particular to describe deuteron-induced reactions [18]. Deuteron-induced reactions are typically modeled as a three-body problem, $n + p + A$, the input being the effective nucleon-target optical potentials. As was later realized, the Coulomb screening method introduced by the Lisbon group [17] could not be applied to deuteron-induced reactions involving heavy targets, due to the increased strength of the Coulomb force [19]. It turns out that, by using a separable representation for the optical potential, those difficulties can be overcome [20]. As a result, in the past few years

*nunes@nscl.msu.edu

separable interactions have made a come back [21–23]. These developments use the Ernst, Shakin, and Thaler scheme (EST) [24] to generate separable representations for the nucleon optical potential.

While most optical potentials being used to interpret nuclear reaction data are local [3,4], separable interactions with realistic truncations are intrinsically nonlocal. Even though at the two-body level the EST scheme ensures that scattering observables are exactly reproduced within a chosen energy range, this is not guaranteed when using these interactions in the context of deuteron-induced reactions, because the three-body equations will pick up off-shell contributions. It has been shown that local and nonlocal optical potentials can give rise to very different transfer cross sections even if they are equivalent at the two-body level [25–28]. It is therefore timely to perform a dedicated study on the effect that the separable EST transformation has on the properties of optical potentials. This is precisely the goal of this work.

We study the scattering of neutrons on two closed-shell nuclei ^{16}O and ^{48}Ca at beam energies of experimental interest and explore the nonlocality properties of the separable interactions in coordinate space. This paper is organized in the following way. In Sec. II we briefly introduce the EST method and the standard Gaussian nonlocality form used to extract the nonlocal parameter for the interaction. In Sec. III we present the results obtained for both targets and discuss these results in the context of previous work. Finally, the conclusions are presented in Sec. IV.

II. THEORETICAL CONSIDERATIONS

Deuteron-induced reactions on intermediate- to heavy-mass targets A are treated as three-body problems consisting of $n+p+A$. In such cases, the three-body dynamics of the reaction is generated from the pairwise interactions: V_{np} reproducing the properties of the deuteron and its continuum, and the nucleon optical potentials U_{nA} and U_{pA}, typically describing nucleon scattering from the target A. In general, these optical potentials are energy dependent and contain an important imaginary term that effectively takes into account the removal of flux from the incident channel into other channels in the reaction that are not explicitly included.

Although there have been many efforts to derive the optical potential from first principles, the common practice is to use a larger set of elastic data to fit it [3,4]. For convenience these potentials are most often made local, although isolated studies have been performed to include nonlocality in these interactions [29]. For simplicity, in this study, we focus on the neutron-target potentials, although the results can be trivially generalized to proton-target potentials.

To construct separable representations of the n-A optical potentials U_{nA}, the generalized EST scheme of [30] is adopted. Although the original EST scheme focused only on Hermitian potentials, the generalization presented in Ref. [30] extends its applicability to potentials that are complex and energy dependent. Because this work focuses only on n-A interactions, we refer to these as U and drop the nA subscript hereafter.

The key features of the generalized EST separable expansion can be summarized as follows. First, one defines the states $|\psi^{(+)}_{E_i}\rangle$ and $|\psi^{(-)}_{E_i}\rangle$, which are eigenstates of the Hamiltonians $H = H_0 + U$ and $H^* = H_0 + U^*$, respectively, with eigenvalues $E_i \geqslant 0$ and H_0 being the free Hamiltonian. The states $|\psi^{(+)}_{E_i}\rangle$ are the usual scattering wave functions fulfilling outgoing boundary conditions, while the asymptotic behavior of $|\psi^{(-)}_{E_i}\rangle$ is that of an incoming spherical wave. Second, the two-body potential U is expanded using the basis states $\{|\psi^{(+)}_{E_i\alpha}\rangle\}$ and $\{|\psi^{(-)}_{E_i\alpha}\rangle\}$, leading to the partial-wave separable potential

$$u_\alpha(E) = \sum_{i,j=1}^{N} |h_{i\alpha}\rangle \lambda^\alpha_{ij}(E) \langle \tilde{h}_{j\alpha}|, \tag{1}$$

where $|h_{i\alpha}\rangle \equiv U_\alpha(E_i)|\psi^{(+)}_{E_i\alpha}\rangle$, $|\tilde{h}_{i\alpha}\rangle \equiv U^*_\alpha(E_i)|\psi^{(-)}_{E_i\alpha}\rangle$, and E is the two-body center-of-mass (c.m.) energy. Here $\alpha \equiv \{l\,j\}$ denotes a single channel, with l being the the orbital angular momentum and $j = |l \pm 1/2|$ the total angular momentum. The number of basis states N defines the rank of the separable potential and the energy eigenvalues E_i are called EST support points. We note that $|h_{i\alpha}\rangle$ and $\langle\tilde{h}_{i\alpha}|$ are related to the half-shell transition (t) matrix by

$$|h_{i\alpha}\rangle = U_\alpha(E_i)|\psi^{(+)}_{E_i\alpha}\rangle = t_\alpha(E_i)|p_i\rangle, \tag{2}$$

$$\langle\tilde{h}_{i\alpha}| = \langle\psi^{(-)}_{E_i\alpha}|U_\alpha(E_i) = \langle p_i|t_\alpha(E_i), \tag{3}$$

where $p_i = \sqrt{2\mu E_i}$ is the on-shell momentum, with μ being the reduced mass. The absolute square of the on-shell t-matrix elements relates directly to the cross section for elastic scattering. The half-shell t matrix elements are obtained in momentum space by solving the Lippmann-Schwinger (LS) equation

$$t_\alpha(E_i)|p_i\rangle = U_\alpha(E_i)|p_i\rangle + U_\alpha(E_i)G_0(E_i)t_\alpha(E_i)|p_i\rangle. \tag{4}$$

Negative-energy EST support points can also be included in the expansion, and in that case the bound-state wave functions replace the incoming and outgoing scattering states (see Ref. [23] for details).

Finally, one defines the coupling matrix $\lambda^\alpha_{ij}(E)$ by imposing the constraint

$$\begin{aligned}\langle\psi^{(-)}_{E_i\alpha}|U_\alpha(E)|\psi^{(+)}_{E_j\alpha}\rangle &= \langle\psi^{(-)}_{E_i\alpha}|u_\alpha(E)|\psi^{(+)}_{E_j\alpha}\rangle \\ &= \sum_{n,m=1}^{N} \langle\psi^{(-)}_{E_i\alpha}|h_{n\alpha}\rangle \lambda^\alpha_{nm}(E) \langle\tilde{h}_{m\alpha}|\psi^{(+)}_{E_j\alpha}\rangle.\end{aligned} \tag{5}$$

This definition of $\lambda^\alpha_{ij}(E)$ ensures that the matrix elements of the original potential $U(E)$ and the separable potential $u_\alpha(E)$ between the basis states are identical for all energies E. For the special case where E corresponds to one of the EST support points, Eq. (5) implies that the eigenstates of $H_0 + u(E_i)$ coincide with those of $H_0 + U(E_i)$. This guarantees that the wave functions obtained using the original potential U are identical to the ones computed with its separable representation u at the EST support points. This is a crucial property of the original EST scheme and is by construction preserved in the generalized expansion for complex potentials.

TABLE I. The EST parameters for the n-^{48}Ca separable potentials. E_{range} specifies the highest support point used, and N is the number of EST support points needed for convergence with a given E_{range}. The specific energies of the support points are shown in the last column; when a range of energy is given, it means that an even spacing of support points within that range were included.

	E_{range} (MeV)	N	Support points E_i (MeV)
EST10-Ca	10	10	0.5 MeV; 0.5–10
EST40-Ca	40	12	0.5, 7 MeV; 7–40
EST400-Ca	400	14	0.5, 10, 30, 60, 100; 100–400
EST800-Ca	800	22	0.5, 10, 30, 60, 100; 100–800
EST1200-Ca	1200	27	0.5, 10, 30, 60, 100; 100–1200
EST1600-Ca	1600	35	0.5, 10, 30, 60, 100; 100–1600
EST2000-Ca	2000	45	0.5, 10, 30, 60, 100; 100–2000
EST2400-Ca	2400	53	0.5, 10, 30, 60, 100; 100–2400

III. RESULTS

We consider the energy-dependent CH89 global optical potential [3] and apply the EST scheme to produce separable forms. We analyze the properties of the resulting potential at two scattering energies, $E = 5$ MeV and $E = 20$ MeV, which span beam energies of experimental interest for applications involving transfer reactions. We consider both the number of support points included in the expansion (the rank N) and the energy range E_{range} for the support points. Support points are chosen wisely based on the structure of the two-body continuum. One can consider that effectively in EST we are interpolating the S matrix $S(E)$ (or T matrix) and, as such, we need to choose the set E_i that will enable the reproduction of the original $S(E)$.

In Table I the specifications of the EST parameters, including the rank used in the expansions and the energies corresponding to the support points, are provided. When a range of energy is given, it means that an even spacing of support points within that range were included. While a rank $N < 10$ is usually sufficient to describe nucleon scattering observables up to 20 MeV, a much higher rank is needed to reach convergence of the potential matrix elements $u_\alpha(r', r)$. Thus we performed calculations up to $N = 53$. We find that the separable interactions obtained depend strongly on the energy range included in the EST procedure. Again, to fully explore this dependence, we consider multiple values of E_{range}, going all the way up to 2400 MeV.

The S matrices generated with the separable interactions agree with those obtained directly with the original CH89 potential within their corresponding energy range but expectedly fail to provide an accurate description outside their energy range. Plotted in Fig. 1 is the real part of the S-matrix resulting from separable interactions with different E_{range}, for s-wave neutrons scattering off ^{48}Ca.

A. Radial dependence of the separable interaction

Next we consider the radial dependence of the separable interactions. While the original CH89 optical potential is local, the resulting separable interactions are nonlocal. To best illustrate this, we present in Figs. 2 and 3 the real part of the n-^{48}Ca separable potential $\text{Re}[u_\alpha(r, r')]$ for $E = 5$ MeV and $E = 20$ MeV, respectively. We show two relevant partial waves ($J^\pi = 1/2^+$ in the left panels and $J^\pi = 3/2^-$ in the right panels) as well as the two extreme cases for the energy range (the lowest $E_{\text{range}} = 10$ MeV on the top and the highest $E_{\text{range}} = 2400$ MeV on the bottom).

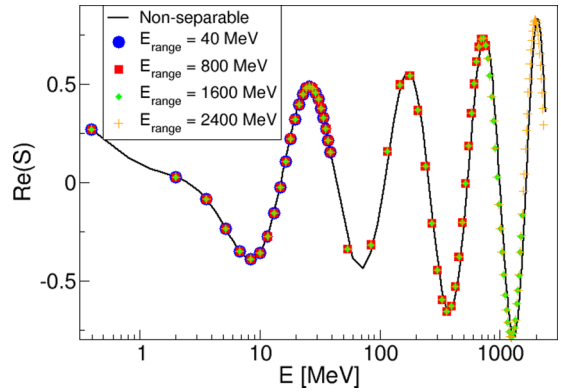

FIG. 1. Real part of the S matrix as a function of the scattering energy for the various energy ranges considered in the EST expansion [example shown for ^{48}Ca(n, n) scattering for $\ell = 0$].

Several characteristics emerge from the analysis.

(i) The separable interactions for $J^\pi = 1/2^+$ and $\ell = 0$ have the minimum at $r = 0$, independently of their rank or energy range. This is shown in panels (a) and (c) of Figs. 2 and 3. Expectedly, introducing the repulsion from the centrifugal barrier shifts the

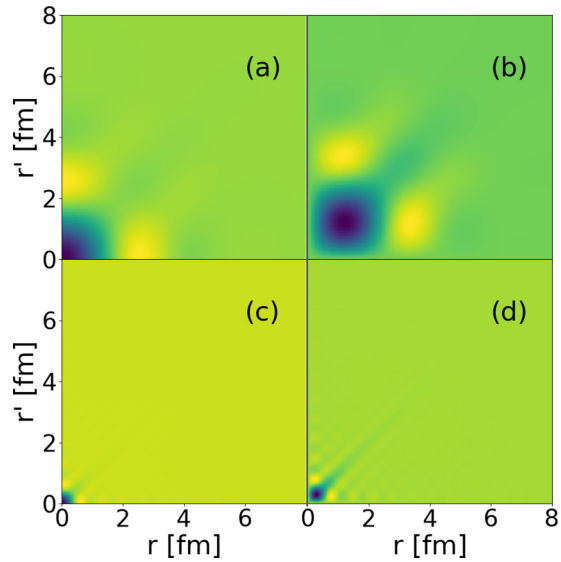

FIG. 2. Radial dependence of the real part of the separable interaction obtained for ^{48}Ca(n, n) at 5 MeV: (a) $J^\pi = 1/2^+$ ($E_{\text{range}} = 10$ MeV), (b) $J^\pi = 3/2^-$ ($E_{\text{range}} = 10$ MeV), (c) $J^\pi = 1/2^+$ ($E_{\text{range}} = 2400$ MeV), and (d) $J^\pi = 3/2^-$ ($E_{\text{range}} = 2400$ MeV). The pale (yellow) and dark (blue) colors correspond to the maxima and minima, respectively. The color scale varies significantly between panels; in this figure we focus only on the geometry of the potentials.

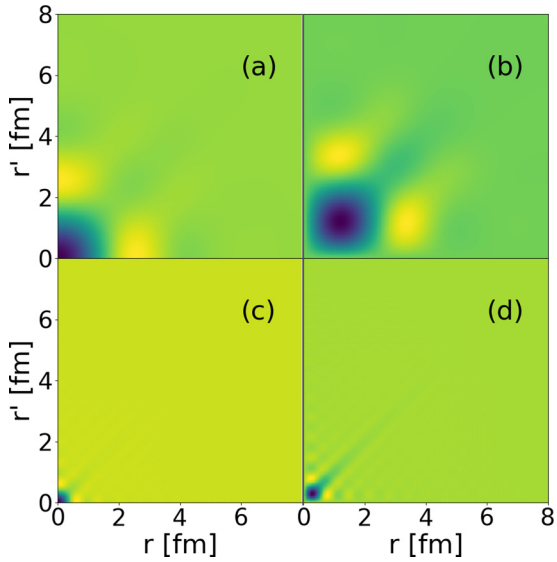

FIG. 3. Radial dependence of the real part of the separable interaction obtained for ^{48}Ca(n,n) at 20 MeV: (a) $J^\pi = 1/2^+$ ($E_{\rm range} = 20$ MeV), (b) $J^\pi = 3/2^-$ ($E_{\rm range} = 20$ MeV), (c) $J^\pi = 1/2^+$ ($E_{\rm range} = 2400$ MeV), and (d) $J^\pi = 3/2^-$ ($E_{\rm range} = 2400$ MeV). The pale (yellow) and dark (blue) colors correspond to the maxima and minima, respectively. The color scale varies significantly between panels; in this figure we focus only on the geometry of the potentials.

minimum of the potential away from $r = 0$ [shown in panels (b) and (d) of Figs. 2 and 3 for the partial wave $J^\pi = 3/2^-$ and $\ell = 1$].

(ii) The potentials with the smaller energy range [shown in panels (a) and (b) of Figs. 2 and 3] have strong off-diagonal components. As we increase the energy range included in the EST procedure, the off-diagonal components shrink gradually toward the diagonal. Ultimately the potentials with the highest energy range [shown in panels (c) and (d) of Figs. 2 and 3] approach the diagonal form of the original CH89 potential.

(iii) The off-diagonal structures of the separable interactions produced for $E = 5$ MeV (Fig. 2) are identical to those obtained for $E = 20$ MeV (Fig. 3). One should keep in mind that CH89 is energy dependent and therefore one might expect the corresponding separable interaction to be energy dependent too. We return to this point in Sec. III C.

The three broad features discussed before are persistent throughout our investigations, whether looking into the real or the imaginary parts of the potential, and whether considering low or high angular momentum ℓ. Also, the separable interactions generated for ^{16}O(n,n) ^{16}O have the same qualitative characteristics as those shown in Figs. 2 and 3.

To best quantify the off-diagonal properties, we consider the separable potential cross diagonals by plotting Re$[u_\alpha(r,r')]$ as a function of $(r-r')$, while fixing $(r+r')$, in the region where the potential has its deep pocket. For $\ell = 1$, we take $(r+r')$ such that the cross-diagonal curve goes through the minimum of each potential. For $\ell = 0$, these minima occur at the origin, so we instead fix $(r+r')$ at 0.4 fm. In Fig. 4 we show the cross-diagonal behavior for the $\ell = 0$ potential for neutrons on ^{48}Ca at 5 MeV. A similar plot is shown in Fig. 5 for $\ell = 1$ neutrons on ^{48}Ca also at 5 MeV.

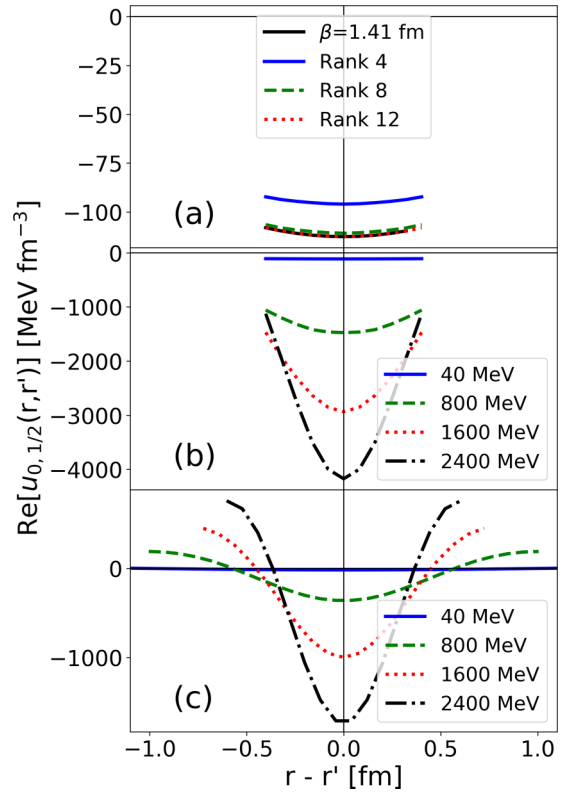

FIG. 4. Cross diagonal of the real part of the separable interaction obtained for ^{48}Ca(n,n) at 5 MeV, $J^\pi = 1/2^+$: (a) comparing different ranks for $E_{\rm range} = 40$ MeV, with $(r+r') = 0.4$ fm, (b) comparing different $E_{\rm range}$ with $(r+r') = 0.4$ fm, and (c) comparing different $E_{\rm range}$ through the potential maxima.

Figures 4(a) and 5(a) show the convergence of the potential with rank for a fixed energy range of $E_{\rm range} = 40$ MeV. Results for $N = 12$ are already converged and the behavior of the cross diagonal in this deep pocket is approximately Gaussian. In contrast, Figs. 4(b) and 5(b) show a very strong dependence of the cross-diagonal potentials with the energy range included when calculating the separable interaction. With increasing $E_{\rm range}$, the interactions become deeper and more localized. In addition, we can analyze the cross-diagonal plots in the surface region when the interaction reaches its maximum [Figs. 4(c) and 5(c)]. The cross-diagonal plots show a strong dependence on the $E_{\rm range}$. This behavior merits further inspection.

B. Nonlocality behavior of the separable expansion

To quantify the nonlocality induced in the interaction we use the form introduced by Perey and Buck [29]. Perey-Buck assume that the nonlocality of the optical potential is Gaussian:

$$U^{\rm PB}(\mathbf{r},\mathbf{r}') = \exp\left(-\left|\frac{\mathbf{r}-\mathbf{r}'}{\beta}\right|^2\right) U_{\rm WS}\left(\frac{\mathbf{r}+\mathbf{r}'}{2}\right), \qquad (6)$$

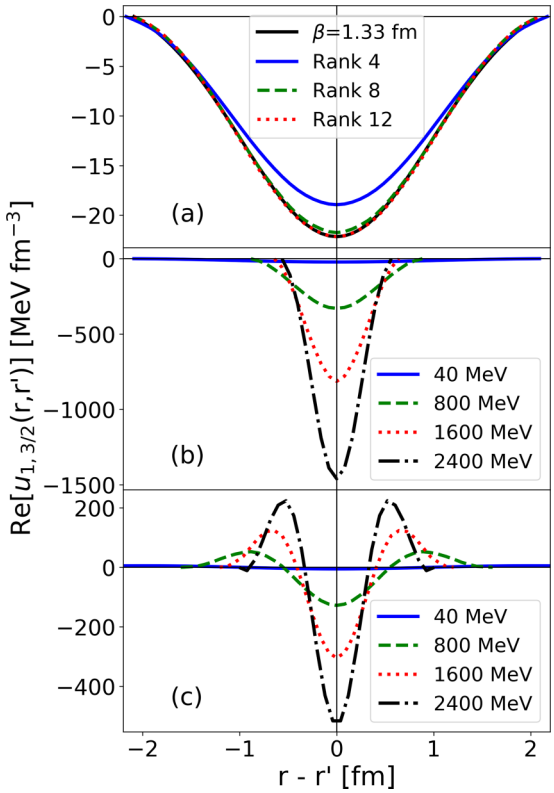

FIG. 5. Cross diagonal of the real part of the separable interaction obtained for ^{48}Ca(n,n) at 5 MeV, $J^\pi = 3/2^-$: (a) comparing different ranks for $E_{\text{range}} = 40$ MeV through the potential minima, (b) comparing different E_{range} through the potential minima, and (c) comparing different E_{range} through the potential maxima.

where U_{WS} is a local Woods-Saxon form and β is the nonlocality parameter.

The partial-wave-decomposed interaction takes the following form (See Ref. [29]):

$$u_\ell^{\text{PB}}(r,r') = \frac{2i^\ell}{\pi^{\frac{1}{2}}\beta} U_{\text{WS}}\left[\frac{1}{2}(r+r')\right] \times j_\ell\left(-i\frac{2rr'}{\beta^2}\right)\exp\left(-\frac{r^2+r'^2}{\beta^2}\right). \quad (7)$$

To quantify the nonlocality, Eq. (7) was used to fit the cross-diagonal shapes of Figs. 4(a) and 5(a) and extract the nonlocality parameter β. In the fits, an arbitrary normalization was chosen and only the cross-diagonal behavior at a fixed $r + r'$ was considered. These fits are shown by the black solid lines in Figs. 4(a) and 5(a) for ^{48}Ca(n,n) at 5 MeV.

We repeat this procedure for each E_{range} considered and find that, consistently, around the minimum, and in the vicinity of $(r - r') = 0$, the separable interaction can be approximated by the functional form in Eq. (7). However, outside the deep pocket of the potential, the behavior is not well represented by the Perey and Buck [29] form and, for that reason, we also study other measures of nonlocality. Particularly, we consider the distance between the innermost roots Δ_{roots} and the distance between the peaks Δ_{peaks} of the interaction, along the cross diagonal in the surface region depicted in Figs. 4(c) and 5(c).

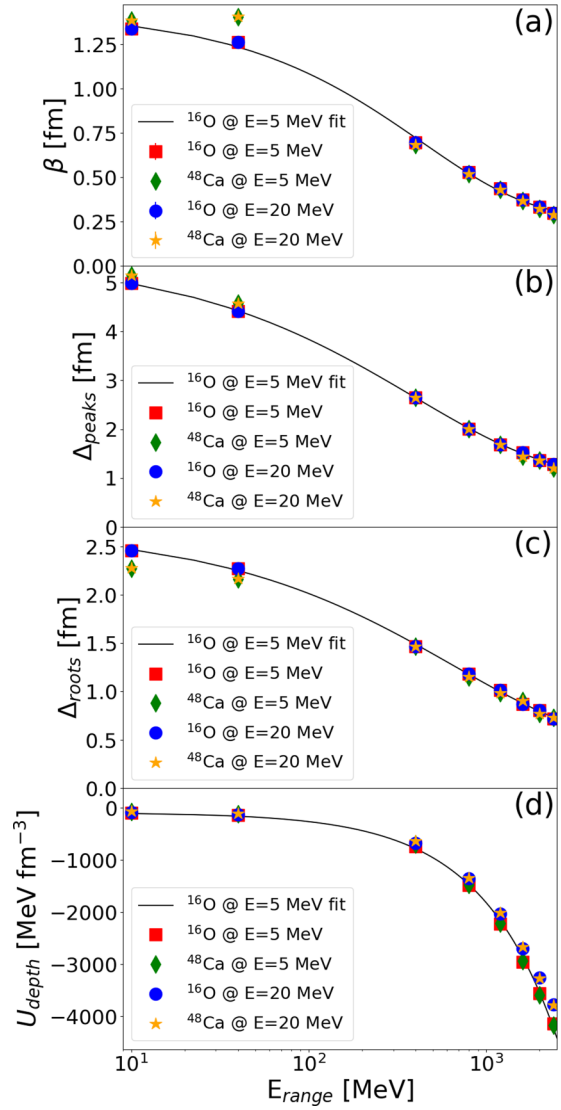

FIG. 6. Nonlocality properties as a function of the energy range for $\ell = 0$ interactions: (a) the nonlocality parameter β, (b) the distance between peaks Δ_{peaks} (fm), (c) the distance between roots Δ_{roots} (fm), and (d) the depth in the minimum U_{depth} (MeV).

The results for β as a function of E_{range} are compiled in Figs. 6(a) and 7(a) for $\ell = 0$ and $\ell = 1$. We include all cases considered, namely neutrons on ^{16}O at 5 MeV (red squares), ^{48}Ca at 5 MeV (green diamonds), ^{16}O at 20 MeV (blue circles), and ^{48}Ca at 20 MeV (yellow stars). The values of β include an error bar corresponding to one standard deviation obtained in the fit. In addition, Figs. 6(b) and 7(b) show the distance between maxima along the cross-diagonal Δ_{peaks} and Figs. 6(c) and 7(c) show the distance between the innermost roots of the potential Δ_{roots} along the cross diagonal taken through the maxima of the potential. Finally, the depth U_{depth}, defined as the minimum along the same cross diagonal as β, is also shown as a function of E_{range} in Figs. 6(d) and 7(d).

We first focus on the energy dependence of the separable potential. Figures 6 and 7 illustrate clearly that results

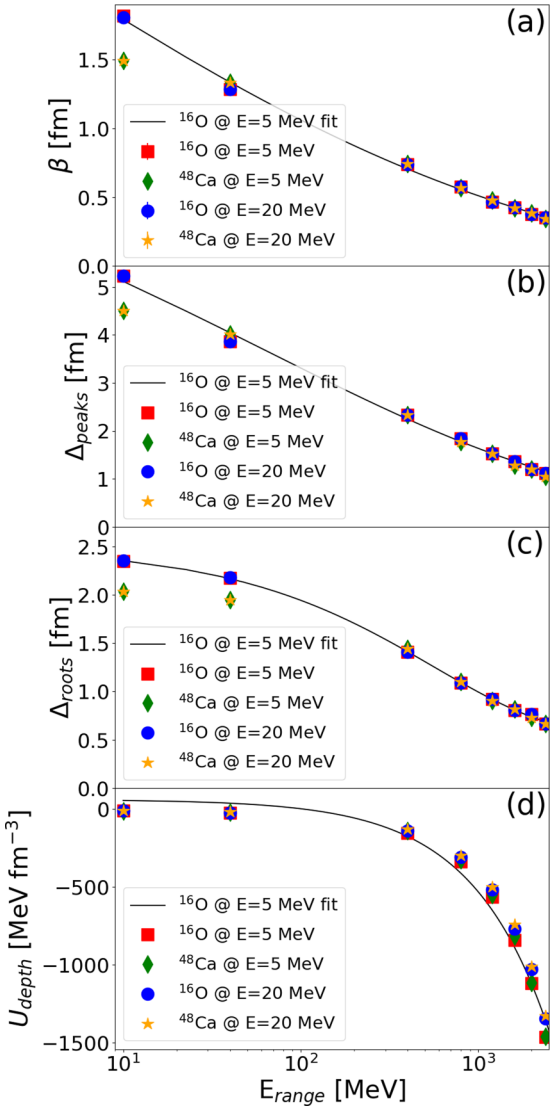

FIG. 7. Nonlocality properties as a function of the energy range for $\ell = 1$ interactions: (a) the nonlocality parameter β, (b) the distance between peaks Δ_{peaks} (fm), (c) the distance between roots Δ_{roots} (fm), and (d) the depth in the minimum U_{depth} (MeV).

for the nonlocal parameters for $E = 5$ MeV are essentially identical to those for $E = 20$ MeV (yellow stars are on top of green diamonds and blue circles are on top of red squares). As mentioned before, this may come as a surprise given that CH89 is strongly energy dependent. However, that energy dependence in the interaction is included through the model space (namely E_{range}) and becomes encoded in the off-diagonal t-matrix terms. It was shown in Ref. [31] (see page 18) that the optical model potential is intrinsically nonlocal and energy-dependent. Imposing locality on the optical potential introduces an additional form of energy dependence. The similarity of the results at 5 and 20 MeV reveals that the intrinsic energy dependence of the optical model potential is weak, which is consistent with the findings of Ref. [30]. In that work it was observed that the t matrices obtained with the energy-independent EST scheme [21] were in close agreement with those obtained with the energy-dependent scheme discussed in Sec. II.[1]

Second, we examine the dependence of the nonlocal behavior of the separable potential with the target. For small values of the energy range, i.e., $E_{\text{range}} < 50$ MeV, the results for ^{16}O differ from those corresponding to ^{48}Ca. This is not surprising because the CH89 potential depends on the mass of the target. However, this difference vanishes as the energy range approaches hundreds of MeV. In fact, for a given channel, the nonlocality is determined exclusively by the energy range. This suggests a universal correlation between the nonlocality and the energy range. To understand how this universality arises we recall that the basis states for the EST expansion are given by the Lippmann-Schwinger equation $|\psi_{E_i}\rangle = |p_i\rangle + G_0(E_i)U(E_i)|\psi_{E_i}\rangle$. The term containing the potential is thus inversely proportional to the energy, so that $|\psi_{E_i}\rangle = |p_i\rangle$ in the limit $E_i \to \infty$. Therefore, the potential should approach a limit that is independent of the details of the original interaction for large energy ranges.

Third, although qualitatively the same, these properties are quantitatively dependent on the partial wave considered. In fact, when increasing the angular momentum, the deviation from the Gaussian form is more pronounced. However, as mentioned before, around the minimum, the Gaussian form is a good approximation.

While the nonlocality parameter varies significantly within the energy ranges considered, one does expect it to go to zero when $E_{\text{range}} \to \infty$ because the original CH89 potential is local. To investigate this, we next consider the functional dependence of $\beta(E_{\text{range}})$ and fit its E_{range} dependence with to two trial functions, the first assuming the behavior is exponential and the second assuming the behavior is a power law:

$$\beta_1(E_{\text{range}}) = a \exp\left(bE_{\text{range}}^c\right) + d, \tag{8}$$

$$\beta_2(E_{\text{range}}) = \frac{a}{(E_{\text{range}} + b)^c} + d. \tag{9}$$

The results for the exponential fit of neutrons on ^{16}O at 5 MeV are plotted in Figs. 6 and 7 (black solid line). As expected, the results are mostly consistent with $\beta(E_{\text{range}} \to \infty) = 0$. However, the rate of convergence differs strongly with angular momentum and is always slower for the partial waves with higher angular momentum. For the other nonlocality measures, the fits [solid black lines in panels (b) and (c) of Figs. 6 and 7] assume the same exponential form as for β, while for

[1]To understand how this occurs, consider an energy-independent nonlocal potential $\tilde{U}(r, r')$ so that $H = H_0 + \tilde{U}$ has the eigenstates ψ_E, with E being the energy eigenvalue. The local potential $U(r)$ that yields the same wave function fulfills $U(r)\psi_E(r) = \int dr' r'^2 \tilde{U}(r, r')\psi_E(r')$. Clearly $U(r)$ must be adjusted for each value of the energy to reproduce the wave functions corresponding to $\tilde{U}(r, r')$, so that $U(r) \equiv U(r, E)$. When the EST scheme is invoked, it seeks to obtain a general nonlocal potential that reproduces the wave functions ψ_E across a whole energy range, although it does not contain the energy dependence induced by localization.

TABLE II. Parameters for the fits of $\beta(E_{\text{range}})$.

E (MeV)	Target	Type	d $(J = 1/2^+)$	d $(J = 3/2^-)$
5	^{16}O	Exponential	0.27 ± 0.05	−0.03 ± 0.60
		Power law	−0.04 ± 0.23	−0.79 ± 0.85
20	^{16}O	Exponential	0.27 ± 0.05	−0.06 ± 0.62
		Power law	−0.04 ± 0.24	−0.86 ± 0.88
5	^{48}Ca	Exponential	0.31 ± 0.06	0.29 ± 0.03
		Power law	−0.09 ± 0.82	−0.07 ± 0.06
20	^{48}Ca	Exponential	0.31 ± 0.06	0.29 ± 0.03
		Power law	−0.09 ± 0.83	−0.07 ± 0.06

the depths [solid black lines in Figs. 6(d) and 7(d)] the fit is linear.

The asymptotic value $\beta(E_{\text{range}} \to \infty) = d$ for all cases here considered are summarized in Table II. Note that in all practical applications used before [23,32], the range considered was $E_{\text{range}} = 50$ MeV, and therefore the potentials would exhibit strong nonlocality.

C. Connection with other frameworks

Now that the properties of the nonlocal separable potentials have been uncovered, it is useful to compare the separable EST to other approaches. We first discuss the assumptions by Perey and Buck [29]. Perey and Buck use a Gaussian form for the nonlocality, estimate the nonlocality parameter to be $\beta = 0.85$ fm, and obtain the remaining parameters of the interaction from fitting angular distributions of neutrons scattering off ^{208}Pb at 7 and 14.5 MeV. The separable interaction we obtain based on a global phenomenological potential for this energy range is $\beta = 0.89$–0.97 fm for $\ell = 0$, consistent with Perey and Buck's assumptions [29]. The value for the nonlocal parameter is significantly larger for higher partial waves, $\beta = 1.46$–1.59 fm for $\ell = 1$. It is important to realize that the original Perey and Buck phenomenological interaction [29] has no energy dependence nor target dependence (except for the standard radius scaling with the mass).

Next we consider microscopic potentials such as those in Refs. [33,34]. These are generated from a truncated many-body framework that effectively imposes an E_{range} in the calculation of the optical potential. Although the behavior of the microscopic optical potential is not Gaussian, the overall shape of $u(r, r')$ cross diagonals for the case of ^{48}Ca [34] are similar to those shown in Fig. 5. The microscopic interaction exhibits $\hat{\beta} \approx 1$ fm. For ^{16}O [33], the cross diagonals are sufficiently different that a quantitative comparison makes no sense. If we used our separable framework to determine the effective energy range included in a given interaction, one would conclude that the microscopic optical potentials of Refs. [33,34] contain physics in the region $E_{\text{range}} < 10$ MeV.

IV. CONCLUSIONS

Because the EST separable method is now being applied to nucleon-nucleus optical potentials for nuclear reaction calculations [21–23], it is important to understand in detail the properties this procedure is inducing in the interactions. Of particular importance is the nonlocality, which has been shown to modify reaction observables. With this goal in mind, we have performed a systematic study, for neutron scattering on two stable targets (^{16}O and ^{48}Ca) at two beam energies $E = 5$ MeV and $E = 20$ MeV. Starting from a local phenomenological optical potential, we have generated separable interactions that represent the neutron scattering process. We have studied the convergence with the rank and the energy range included in constructing the interaction.

We find that the separable procedure induces a large nonlocality in the interaction when $E_{\text{range}} < 50$ MeV. Moreover, we observe that, even when including in the expansion many support points with energy ranges up to $0 \leqslant E \leqslant 2400$ MeV, the resulting potential retains nonlocal behavior. This nonlocality becomes considerably smaller as E_{range} is increased, eventually tending to zero as $E_{\text{range}} \to \infty$ as expected. While for small E_{range} the magnitude of the nonlocality depends on the target, this dependence is washed away for increasing E_{range}, following a universal curve. Focusing on the deep pocket of the separable interaction, for all cases we find that the nonlocality increases with angular momentum.

While there is a strong dependence of the separable optical potential with E_{range} used to construct it, there is virtually no dependence on the beam energy. The strong energy dependence in the original phenomenological optical potential disappears once nonlocality is allowed in the interaction.

We also compare our results with other studies on nonlocal optical potentials. We find that overall the separable interactions are not well described by the Gaussian form used by Perey and Buck [29]. However, around the minimum, they can be approximated by a Gaussian form, and for s waves the magnitude of nonlocality we obtain is similar to that assumed by Ref. [29]. We also compare our interactions for ^{48}Ca with those obtained from *ab initio* calculations [34].

In closing, it is useful to think about the EST procedure in the context of renormalization group theory. In Ref. [9], the effective potential is defined through the Block-Horowitz equation. This equation explicitly resums all the higher-momentum modes while preserving the low-energy momentum scattering amplitudes. Because the effective interaction produced this way is energy dependent, another transformation is needed to arrive at an interaction that is only momentum-dependent $V_{\text{low}k}(k, k')$. A direct comparison between EST and $V_{\text{low}k}$ is currently not possible (because $V_{\text{low}k}$ has not been applied to optical potentials) but could be very enlightening. For both the EST and $V_{\text{low}k}$ schemes, the potentials are constrained so that the bound and scattering states of the original interaction are reproduced over a finite energy range. As such, both techniques have the effect of shuffling high-momentum components into nonlocal behavior of the effective interaction.

ACKNOWLEDGMENTS

We thank Scott Bogner and Charlotte Elster for useful discussions. This work was supported by the National Science Foundation under Grant No. PHY-1811815. This work relied on iCER and the High Performance Computing Center at Michigan State University for computational resources.

[1] R. Machleidt and I. Slaus, J. Phys. G: Nucl. Part. Phys. **27**, R69 (2001).
[2] P. E. Hodgson, Rep. Prog. Phys. **47**, 613 (1984).
[3] R. Varner, W. Thompson, T. McAbee, E. Ludwig, and T. Clegg, Phys. Rep. **201**, 57 (1991).
[4] A. Koning and J. Delaroche, Nucl. Phys. A. **713**, 231 (2003).
[5] R. B. Wiringa, V. G. J. Stoks, and R. Schiavilla, Phys. Rev. C **51**, 38 (1995).
[6] D. Thompson, M. Lemere, and Y. Tang, Nucl. Phys. A **286**, 53 (1977).
[7] R. Machleidt and F. Sammarruca, Eur. Phys. J. A **56**, 95 (2020).
[8] S. Bogner, T. Kuo, and A. Schwenk, Phys. Rep. **386**, 1 (2003).
[9] S. Bogner, T. Kuo, A. Schwenk, D. Entem, and R. Machleidt, Phys. Lett. B **576**, 265 (2003).
[10] S. K. Bogner, R. J. Furnstahl, and R. J. Perry, Phys. Rev. C **75**, 061001(R) (2007).
[11] J. Haidenbauer and W. Plessas, Phys. Rev. C **30**, 1822 (1984).
[12] Y. Koike, J. Haidenbauer, and W. Plessas, Phys. Rev. C **35**, 396 (1987).
[13] W. Plessas, Three-body problem with separable-expansion techniques and use of modern nucleon-nucleon forces, in *Models and Methods in Few-Body Physics*, Lecture Notes in Physics Vol. 273, edited by L. S. Ferreira, A. C. Fonseca, and L. Streit (Springer, Cham, Switzerland, 1987), pp. 137–160.
[14] E. Alt, P. Grassberger, and W. Sandhas, Nucl. Phys. B **2**, 167 (1967).
[15] I. Fachruddin, C. Elster, and W. Glöckle, Phys. Rev. C **62**, 044002 (2000).
[16] H. Witała and W. Glöckle, Phys. Rev. C **85**, 064003 (2012).
[17] A. Deltuva, A. C. Fonseca, and P. U. Sauer, Phys. Rev. C **71**, 054005 (2005).
[18] A. Deltuva and A. C. Fonseca, Phys. Rev. C **79**, 014606 (2009).
[19] N. J. Upadhyay, A. Deltuva, and F. M. Nunes, Phys. Rev. C **85**, 054621 (2012).
[20] A. M. Mukhamedzhanov, V. Eremenko, and A. I. Sattarov, Phys. Rev. C **86**, 034001 (2012).
[21] L. Hlophe, C. Elster, R. C. Johnson, N. J. Upadhyay, F. M. Nunes, G. Arbanas, V. Eremenko, J. E. Escher, and I. J. Thompson (TORUS Collaboration), Phys. Rev. C **88**, 064608 (2013).
[22] L. Hlophe, V. Eremenko, C. Elster, F. M. Nunes, G. Arbanas, J. E. Escher, and I. J. Thompson (TORUS Collaboration), Phys. Rev. C **90**, 061602(R) (2014).
[23] L. Hlophe, J. Lei, C. Elster, A. Nogga, and F. M. Nunes, Phys. Rev. C **96**, 064003 (2017).
[24] D. J. Ernst, C. M. Shakin, and R. M. Thaler, Phys. Rev. C **8**, 46 (1973).
[25] A. Ross, L. J. Titus, F. M. Nunes, M. H. Mahzoon, W. H. Dickhoff, and R. J. Charity, Phys. Rev. C **92**, 044607 (2015).
[26] A. Ross, L. J. Titus, and F. M. Nunes, Phys. Rev. C **94**, 014607 (2016).
[27] L. J. Titus, F. M. Nunes, and G. Potel, Phys. Rev. C **93**, 014604 (2016).
[28] W. Li, G. Potel, and F. Nunes, Phys. Rev. C **98**, 044621 (2018).
[29] F. Perey and B. Buck, Nucl. Phys. **32**, 353 (1962).
[30] L. Hlophe and C. Elster, Phys. Rev. C **93**, 034601 (2016).
[31] H. Feshbach, Annu. Rev. Nucl. Part. Sci. **8**, 49 (1958).
[32] J. Lei, L. Hlophe, C. Elster, A. Nogga, F. M. Nunes, and D. R. Phillips, Phys. Rev. C **98**, 051001(R) (2018).
[33] J. Rotureau, P. Danielewicz, G. Hagen, F. M. Nunes, and T. Papenbrock, Phys. Rev. C **95**, 024315 (2017).
[34] J. Rotureau, P. Danielewicz, G. Hagen, G. R. Jansen, and F. M. Nunes, Phys. Rev. C **98**, 044625 (2018).